Influence of hydrodynamic interactions on the productivity of PeWEC wave energy converter array

Proc. of the International Conference on Electrical, Computer, Communications and Mechatronics Engineering (ICECCME)
16-18 November 2022, Maldives

2022 International Conference on Electrical, Computer, Communications and Mechatronics Engineering (ICECCME) | 978-1-6654-7095-7/22/$31.00 ©2022 IEEE | DOI: 10.1109/ICECCME55909.2022.9988093

Influence of hydrodynamic interactions on the productivity of PeWEC wave energy converter array

Francesco Niosi
MOREnergy Lab, DIMEAS
Politecnico di Torino
Turin, Italy
0000-0002-5105-3482

Beatrice Battisti
MOREnergy Lab, DIMEAS
Politecnico di Torino
Turin, Italy
0000-0001-5918-6055

Sergej Antonello Sirigu
MOREnergy Lab, DIMEAS
Politecnico di Torino
Turin, Italy
0000-0001-5192-5220

***Abstract*—The deployment of multiple Wave Energy Converters in wave farms is the necessary step for wave energy to become competitive with respect to the other renewable energy sources. The numerical simulation of such arrays is complex because of the interaction among the devices, especially for converters characterized by multiple degrees of freedom. In this paper, the influence of two PeWECs (Pendulum Wave Energy Converters) is analyzed, at different positions with respect to the incoming waves. The perturbed wave field and the productivity of the array is investigated in comparison to the single device case in several configurations.**

***Index Terms*—Wave Energy Converters, Array, Hydrodynamics, Annual Energy Production, Wave Scatters.**

I. Introduction

Renewable energy plays a key role in the current climate crisis and geopolitical scenario [1]. Among the different renewable energies, wave energy has a high energy density and predictability [2], but is far behind in its development with respect to the other sources like photovoltaic and wind and accurate design tools are required to have a proper estimate of the WECs productivity given the site of deployment [3]. Different types of Wave Energy Converters (WECs), such as point absorber [4] or ISWEC devices [5], are being studied and analyzed and for the reduction in the cost of energy and power production at commercial scale, WECs need to be deployed in arrays. Wave farms of floating devices have not reached the sea yet, and their numerical simulations are rare, mainly applied to point absorbers. In addition to the large size of the simulations, the description of the hydrodynamics involved in the arrays in nontrivial. Indeed, the WECs interact and have a significant impact on the surrounding area, and thus, their layout should be carefully analyzed. In this paper, the influence of two PeWECs (Pendulum Wave Energy Converters) on their power production is assessed and the perturbed wave field observed. PeWEC is a rotating mass device, characterized by a floating hull containing a pendulum, which, because of its relative rotation with respect to the shaft of an electrical generator, is responsible for the power production. The device is 14.8 m long, 22.5 m wide and 7.4 m high, it is moored to the seabed using a spreading catenary [6], that allows it to align the pitch degree of freedom with the waves. A graphical scheme of PeWEC can be found in Figure 1 and a more detailed description of the mooring system in [7] and [6].

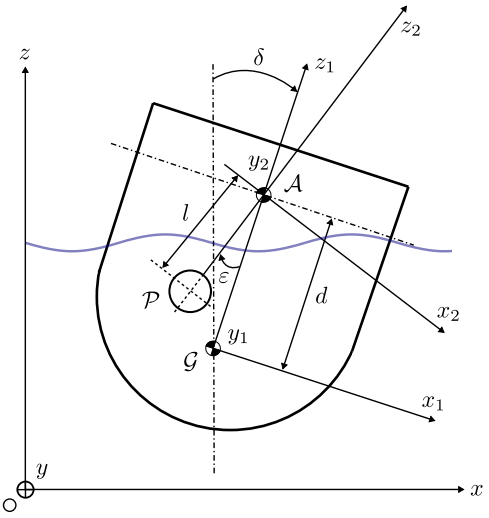

Fig. 1. Scheme of PeWEC device.

For the numerical simulations, the potential theory software NEMOH [8] is chosen as the best trade-off between accuracy and computational cost. Developed at Ecole Centrale de Nantes, NEMOH is an open source Boundary Element Methods (BEM) code used for the calculation of the hydrodynamic coefficients and the free surface elevation. It is also used for the computation of the diffraction transfer matrix and radiation characteristics [9], which are extremely useful for the assessment of the behavior of a wave farm, and its optimization. In this work, we want to characterize the mutual influence of two devices as a function of their spatial position. This is critical for understanding which is the best trade-off for

*Corresponding author: francesco.niosi@polito.it This research has received funding from the Italian National Agency for New Technologies, Energy and Sustainable Economic Development (ENEA), under the project PTR-PTR 19 21 ENEA PRG 7.

placing WECs. By reducing the distance between them, you can save on the costs of the mooring system, electrical cables and maintenance, but it is necessary to understand how this distance affects their productivity. To achieve this goal, this article carries out a preliminary study on the hydrodynamic interaction of the devices and the productivity for different reciprocal positions is calculated. The paper is organized as follows. In Section II, the theory implemented in NEMOH is recalled. The numerical simulations of a single body and an array of two devices are presented in Section III, and the analysis of the productivity in the two cases is carried out in Section IV. Conclusions are then drawn in Section V.

II. Theory

Potential flow theory is based on the assumptions that the fluid is inviscid and incompressible, the flow is irrotational and thus there exists a velocity potential $\Phi(\mathbf{x},t) = \mathrm{Re}[\phi(\mathbf{x})\,\mathrm{e}^{\mathrm{i}\omega t}]$, which satisfies Laplace's equation $\nabla^2\phi = 0$ everywhere in the domain, with ω the angular wave frequency, and $(\mathbf{x},t)$ the spatial and temporal variables, respectively. To further simplify the problem, linearizing assumptions can be done such as small amplitude motions of the body and small wave amplitude.

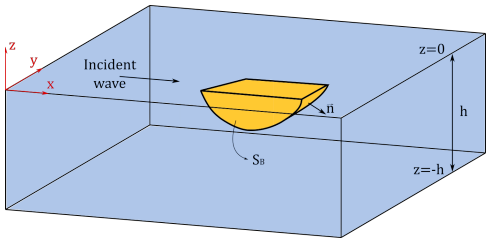

Fig. 2. Outline of the fluid domain for the potential flow theory.

In Fig. 2, the fluid domain for the potential flow theory is outlined, with the reference system.

1) The free surface elevation: The velocity potential can be decomposed in three elements: the incident potential ϕ^I, the diffraction potential ϕ^D and the radiation potential ϕ^R, and their sum gives the perturbed potential ϕ^P, as in (1).

$$\phi^P = \phi^I + \phi^D + \mathrm{i}\omega \sum_{q=1}^{N_{DOF}} \zeta_q \phi_q^R. \tag{1}$$

In particular, the radiated potential is due to the motions for the N_{DOF} degrees of freedom of the body. ζ_q is the Response Amplitude Operator (RAO) of the q-th degree of freedom, obtained from the equation of motion [10]:

$$[-\omega^2(\mathrm{M} + \mathrm{A}(\omega)) + \mathrm{i}\omega\mathrm{B}(\omega) + \mathrm{C}]\zeta(\omega) = \mathrm{F}(\omega). \tag{2}$$

In (2), M is the body mass matrix, A is the added mass matrix, B the added damping matrix, C the matrix of hydrostatic and gravitational restoring coefficients, and F represents the external excitation forces.

The incident potential of a wave of unitary amplitude, travelling in the direction β, is defined as:

$$\phi^I = \mathrm{i}\frac{g}{\omega} f_0\, \mathrm{e}^{-\mathrm{i}k_0(x\cos\beta + y\sin\beta)}, \tag{3}$$

where k_0 is the angular wave number $k_0 = \frac{2\pi}{\lambda}$, with λ as the wavelength, and

$$f_0 = \frac{\cosh k_0(h+z)}{\cosh k_0 h}.$$

The form of the diffraction and radiation potentials is derived from the far-field approximation:

$$\phi^D, \phi_q^R \sim \mathrm{i}\frac{g}{\omega} f_0 \frac{\mathcal{K}(\theta)}{\sqrt{k_0 r}}\, \mathrm{e}^{-\mathrm{i}k_0 r}, \tag{4}$$

where r is the radius of the fictitious circular-cylinder around the body and $\mathcal{K}(\theta)$ is the Kochin function, which depends on the direction θ, and is defined as in [11], and is one of the outputs of the NEMOH solver.

Finally, the free surface elevation is derived from the expression:

$$\eta = -\mathrm{i}\frac{\omega}{g}\phi|_{z=0}. \tag{5}$$

2) The Boundary Value Problem: The boundary conditions to the Laplace's equation are the following:

$$\begin{aligned}
&\frac{\partial\phi}{\partial z} - \frac{\omega^2}{g} = 0 && z = 0,\\
&\frac{\partial\phi}{\partial z} = 0 && z = -h,\\
&\phi^D, \phi_q^R \propto \frac{\mathrm{e}^{-\mathrm{i}k_0 r}}{\sqrt{k_0 r}} && k_0 r \to \infty,\\
&\frac{\partial\phi^I}{\partial n} + \frac{\partial\phi^D}{\partial n} = 0 && \text{on } S_B,\\
&\frac{\partial\phi_q^R}{\partial n} = \mathrm{i}\omega \mathrm{n}_q && \text{on } S_B,
\end{aligned} \tag{6}$$

3) Power Production: The estimation of the productivity of the device combines the WEC's power matrix and the wave scatter diagram for a given site, which give significant wave amplitudes H_s and energetic periods T_e, as well as the distribution of the sea states occurrence $\mathcal{O}$.
The Gross Power is calculated for each wave in the scatter diagram as [11]:

$$P_{Gross} = \frac{1}{2}\omega^2 \mathrm{c} H_s |\zeta_p|^2, \tag{7}$$

where c is the pendulum damping, a control parameter which varies for each wave, and $|\zeta_p|$ is the pendulum RAO, intended as the rotation of the pendulum over the wave height.

Once the Gross Power is computed for each wave, the total Net Power is calculated by subtracting to the Gross Power the Loss of the Power Take-Off system (PTO) and the Base Load Losses due to electric components, the last ones being fixed constant losses. In order to estimate the total energy production of a device over a year, the Net Power related to each wave is

interpolated over the wave scatter diagram and computed over the time period, defined as $\Delta T = 365\,\text{days} \times 24\,\text{hours/day}$. In this way, the Total Net Productivity over a year can be obtained [12]:

$$P_{Net} = \sum_{n=1}^{N_{waves}} P_{Net_n} \mathcal{O}_n \Delta T. \tag{8}$$

4) Application to a Wave Farm: When compared to other numerical methods like CFD (Computational Fluid Dynamics), BEM solvers are less accurate but considerably faster. The computational efficiency of the BEM solver NEMOH makes it suitable for the simulation of multiple bodies, in particular for optimization routines and preliminary array studies [4]. In the case of an array of N bodies, the matrices in (2) will increase in dimensions, and the radiation potential will have to consider $N \times N_{DOF}$ degrees of freedom.
In this paper, simulations for two devices give preliminary results on their impact on the productivity and the perturbed wave field. Adding more devices would increase drastically the computational cost, also because of the complexity of the WEC considered. For this reason, the methodology proposed in [9] for the calculation of the hydrodynamics operators known as Diffraction Transfer Matrix (DTM) and Radiation Characteristics (RC) will be implemented in order to accelerate the simulations. Consequently, an optimization study on the farm layout will be computationally acceptable.

III. Numerical Simulations

Since the hydrodynamic interaction among hulls affects the farm productivity, the numerical simulations chosen in this study aim at characterizing the productivity of two hulls placed at a defined distance, multiple of the device length along X direction, and for different relative orientations. Therefore, the following simulations are performed:

- Single body simulation. Number of simulations:1.
- Two-bodies simulations, placed at a distance equal to 3L, and orientations: 0° (case A), 45° (case B), 90° (case C) with respect to the X direction, as shown in Fig. 3. Number of simulations:3.
- Two-bodies simulations, placed at a distance equal to 6L, and orientations: 0° (case A), 45° (case B), 90° (case C)with respect to the X direction, as shown in Fig. 3. Number of simulations:3.

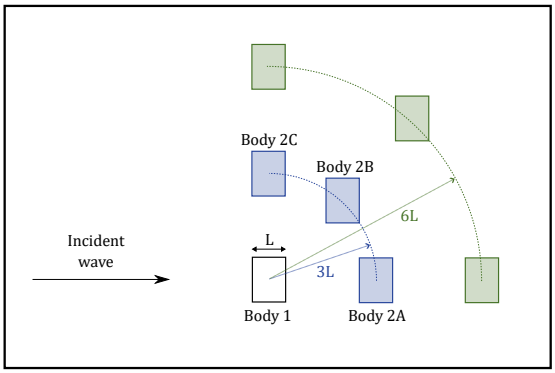

Fig. 3. Layout of the two-bodies array, in the three configurations considered in the study.

A. Single Body Simulations

Through the open-source software Nemoh [8] it is possible to calculate the RAOs referred to the CoG of the hull and characterize the free surface elevation. The considered device is optimized through a genetic algorithm according to the procedure highlighted in [13]. Due to its design, the device radiates and diffracts waves mainly due to its pitching motion. In Figure 4 and Figure 5 are reported respectively a representation of the mesh used for the calculation (of both single body and multi body calculation) and the results regarding the total Free Surface Elevation (FSE) of the single body. The mesh was selected downstream of a convergence study by choosing the best compromise that provides good results with minimum computational time. As a term of comparison, the "Normalised Root Mean Square Error Goodness of Fit (GoF)" is calculated between the values of Added Mass, Damping, LoadRAO and RAOs for the pitching motion related to the benchmark mesh with 3294 panels. The mesh is generated generated as a function of the ratio $r = \lambda_{wavemin}/L_{panel}$. The selected mesh has 1007 panels and ensures a GoF min above 90% with respect to the benchmark and a computational time of 80 min considering: 41 frequencies, one wave direction $\beta = 0$, Kochin functions calculation from $0°$ to $360°$ each $1°$, FSE calculation for a grid with $200x200$ points, a GMRES (Generalized Minimal Residual Method) solver type with tolerance 5e-7. Deactivating the calculation of the free surface and Kochin functions instead it employs 6.15 minutes.

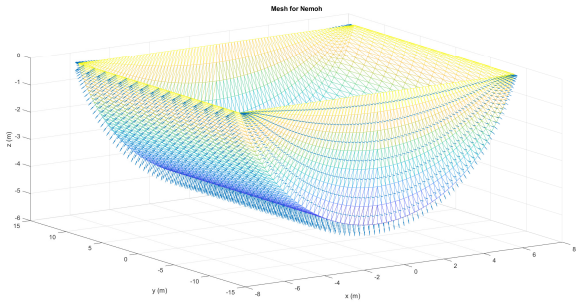

Fig. 4. Visualization of the Mesh used for BEM computation

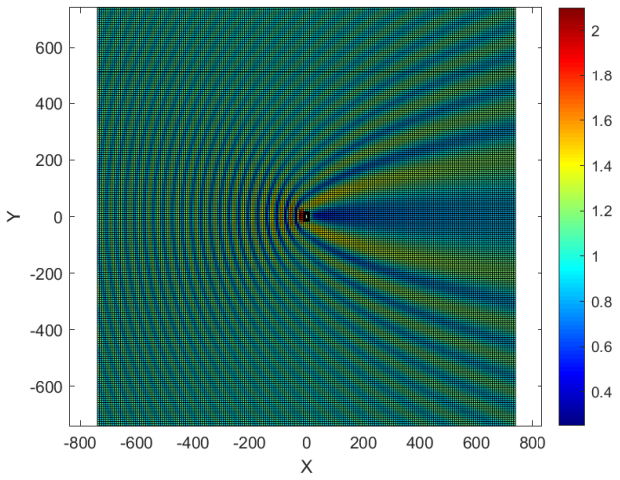

Fig. 5. Free Surface Elevation for single body simulation at frequency $\omega = 0.9593 rad/s$

B. Two-Bodies Simulations

When considering multiple bodies within the BEM calculation, the size of hydrodynamic matrices become $6 \cdot nDOF x 6 \cdot nDOF$ where the non-diagonal terms model the interaction between the bodies. By solving the equation of motion (2) in the frequency domain, it is possible to obtain the RAOs of the devices. The pitch RAOs obtained for the aforementioned configurations are shown below in Figure 6, Figure 7 and Figure 8.

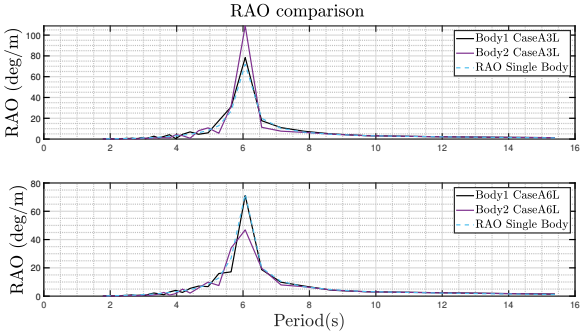

Fig. 6. Hydrodynamic Pitch RAO Case A

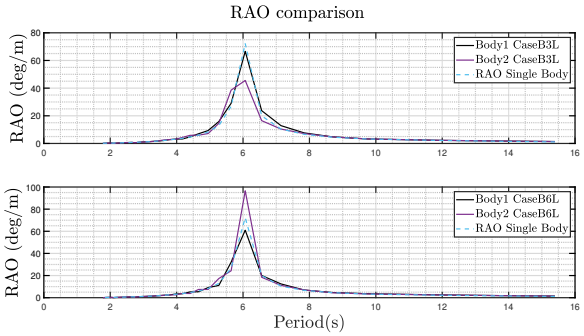

Fig. 7. Hydrodynamic Pitch RAO Case B

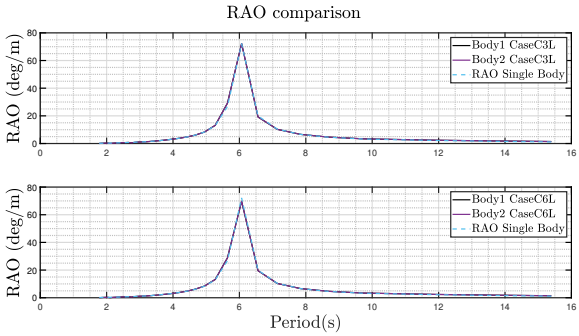

Fig. 8. Hydrodynamic Pitch RAO Case C

IV. Productivity Analysis

For each of the seven simulations, each device productivity is computed following the procedure described in II-3, and considering the yearly wave scatter of Pantelleria (Fig. 9), a small island in the south-west of Italy, where wave energy systems are fundamental for the energy production.

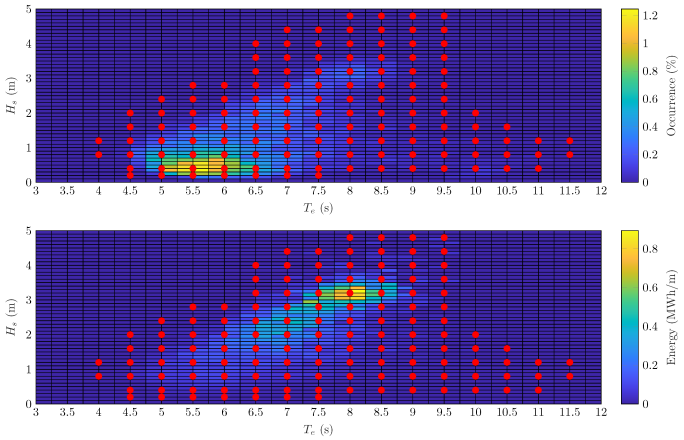

Fig. 9. Scatter diagram of Pantelleria Island.

The wave scatter diagram is obtained from a numerical evaluation of the wave energy resource, for a period of one year. The set of representative waves for productivity is chosen in order to adequately cover areas of the scatter diagram with non-negligible occurrence as can be seen in Figure 9. It is important to specify that the productivity is calculated considering that the pendulum is controlled through the parameters c and k according to the procedure depicted in [14] for the analogous ISWEC device, which are optimized for each wave. In the case of multibody, single-body optimized control parameters c and k are used for both devices. Obviously this is not the best procedure. In fact, the control parameters c and k should be optimized [15] taking into account the presence of more bodies. Given that at the moment, the purpose of the paper is to characterize the hydrodynamic interaction between the devices and not to maximize the energy produced, we proceeded with this assumption. When the productivity of the device wants to be calculated, the pendulum is coupled to the

hull and the equation of motion in frequency domain of the complete system referred to the single body reads as follow:

$$\left(-\omega^2 \cdot \begin{bmatrix} M_{1,1}(\omega) & \cdots & M_{1,5}(\omega) & \cdots & 0 \\ \vdots & \ddots & \vdots & \vdots & \vdots \\ M_{5,1}(\omega) & \cdots & M_{5,5}(\omega) & \vdots & 0 \\ \vdots & \vdots & \vdots & \ddots & \vdots \\ -m_pL & \cdots & (I_p + m_pL^2 - m_pLd) & \cdots & I_p + m_pL^2 \end{bmatrix} + \right.$$

$$+i \cdot \omega \begin{bmatrix} B_{1,1}(\omega) & \cdots & B_{1,5}(\omega) & \cdots & 0 \\ \vdots & \ddots & \vdots & \vdots & \vdots \\ B_{5,1}(\omega) & \cdots & B_{5,5}(\omega) & \vdots & 0 \\ \vdots & \vdots & \vdots & \ddots & \vdots \\ 0 & \cdots & \cdots & \cdots & c(\omega) \end{bmatrix} + \tag{9}$$

$$\left. + \begin{bmatrix} K_{1,1} & \cdots & K_{1,5} & \cdots & 0 \\ \vdots & \ddots & \vdots & \vdots & \vdots \\ K_{5,1} & \cdots & K_{5,5} & \vdots & m_pgL \\ \vdots & \vdots & \vdots & \ddots & \vdots \\ 0 & \cdots & \cdots & \cdots & k(\omega) + m_pgL \end{bmatrix} \right) \begin{Bmatrix} \zeta_1(\omega) \\ \zeta_2(\omega) \\ \vdots \\ \zeta_7(\omega) \end{Bmatrix} = \begin{Bmatrix} F_{ex1}(\omega) \\ F_{ex2}(\omega) \\ \vdots \\ 0 \end{Bmatrix}$$

where $M_{i,i}$ is the device mass or inertia (including the pendulum) plus the frequency dependent added mass relative to the considered DoF,I_p is the pendulum inertia and m_p its mass, L is the pendulum length, d is the distance between the device centre of gravity (CoG) and the pendulum fulcrum, $B_{i,i}$ is the radiation damping related to the hull, c is the PTO damping, $K_{i,i}$ is the hydrostatic stiffness of the hull and k is the PTO stiffness term. All the terms related to the pendulum are reported in blue inside the matricial equation. Solving the 7DoF equation of motion, the pendulum rotation ζ_7 can be obtained, thus the productivity calculated. In the case of two bodies, the equation of motion becomes a system with 14 degrees of freedom in which the lines and columns 7 and 14 refer to the coupling with the pendulum characterized by the control parameters c and k. Once the pendulum RAO is obtained, the productivity can be calculated according to Eq.8. As described in Section III, six different multibody configuration have been analyzed in this study and the associated productivity results are depicted in Figure 6, Figure 7 and Figure 8. Remembering that in this case we are considering a frontal wave and that the device pitches around the y axis, perpendicular to the wave direction, most of the radiation of the device will be emitted precisely because of the pitching motion thus, Case A, in which the devices are placed along the wave direction, becomes the most interesting to analyze. As highlighted in Figure 10, when the hulls are placed at a distance equal to three times the device length, the productivity of both devices is strongly affected. Instead, when the devices are placed at a major distance only the productivity of the second device (Figure 3) is consistently affected. In both the other cases, shown in Figure 11 and Figure 12 when the distance between the devices is equal to 6L, their productivity is not modified. In case C, this happens also for a distance equal to 3L. In the previously mentioned figures it can be seen how, for some simulations the productivity of a device can exceed the one of the single body. This is possible and is due to the constructive interference between radiated wave, diffracted wave and incident wave.

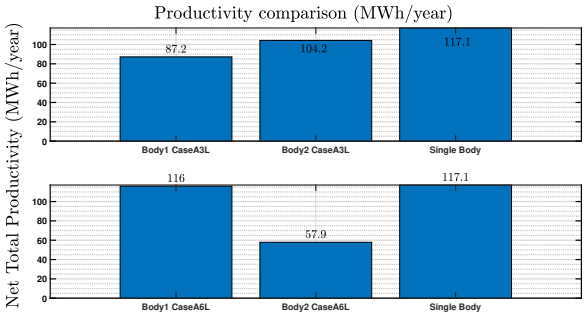

Fig. 10. Net Productivity Case A

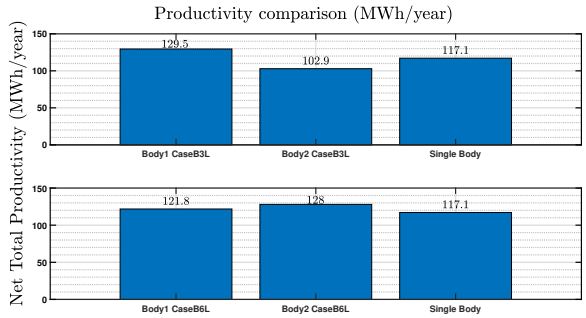

Fig. 11. Net Productivity Case B

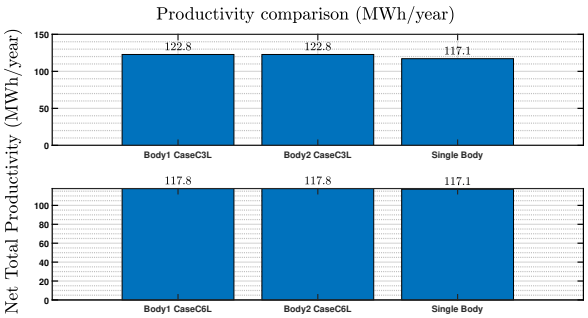

Fig. 12. Net Productivity Case C

Since it was found that for cases B and C, for a distance equal to 6L, the two devices no longer affect each other, while for case A this continues to happen, we conducted a further analysis relating to Case A by varying the distance up to $20L$. In Figure is reported the factor q as a function of the distance between the two devices. The factor q is defined as follow:

$$q = \frac{AEP_a}{n \cdot AEP_s} \tag{10}$$

where AEP_a is the Annual Energy Production of the array while AEP_s is related to the the single isolated device, and n

is the number of units in the array. As can be seen in Figure 13, at certain distances the array AEP decreases with respect to the isolated devices. This happens at a distance $d = 3L$ and $d = 6L$. This phenomenon is related to the geometrical and inertial characteristic of the analysed device. At certain wave frequencies, radiated, diffracted and incident potentials combine themselves strongly affecting the wave field. In Figure 14 is reported a visualization of the amplitude of the total free surface elevation related to an incident wave of amplitude 1m. The Figure shows two configurations ($d = 20L$ and $d = 3L$) considering a wave with frequency of $0.9593 rad/s$ which is close to the resonant frequency of the PeWEC. It can be noticed that when the devices are near, the wave amplitude strongly varies in the area close to the devices.

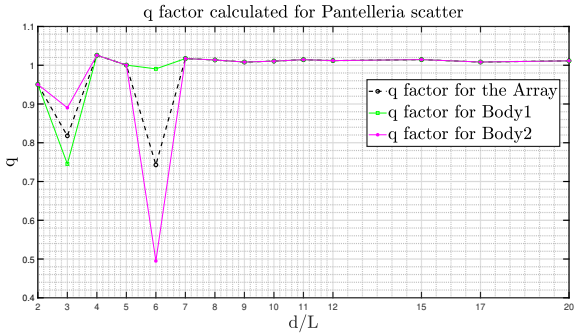

Fig. 13. q factor calculated for Array configuration, for Body 1 and for Body 2 for different distances d

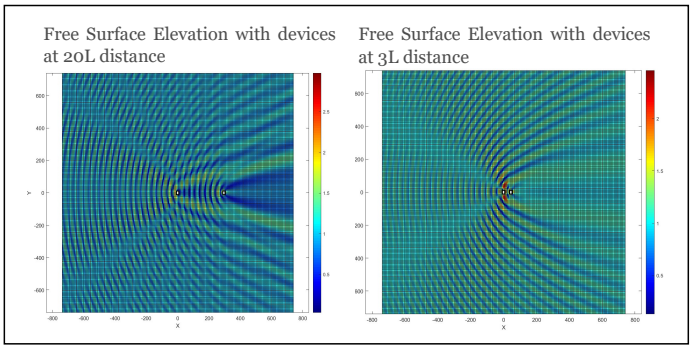

Fig. 14. Qualitative representation of the free surface for two configurations with devices at a distance equal to 3L and 20L

V. Conclusions and Future Works

The results obtained in this work show that it is necessary to consider the hydrodynamic interaction between floating bodies when planning an installation of WEC farms. Since as the number of bodies to model increases, the computational cost increases considerably, it is necessary to streamline the calculation to proceed with the optimization of the arrangement of WECs within the farm. To do this we will proceed with the implementation of the interaction theory proposed by MacNatt [11] and we will compare the results obtained through BEM. The advantage of the interaction theory is that it is enough to model a single device and, given that all the WECs in the farm are the same, numerically transport the hydrodynamic interaction without solving the BEM for the other bodies. Finally, it should be emphasized that the results obtained relating to the AEP are referred to a non-optimized control. We will proceed with the implementation of controllers for farms as suggested in [16].

References

[1] G. Mattiazzo, "State of the art and perspectives of wave energy in the mediterranean sea: Backstage of iswec," *Frontiers in Energy Research*, vol. 7, 2019. Cited by: 26; All Open Access, Gold Open Access, Green Open Access.

[2] B. Guo and J. V. Ringwood, "Geometric optimisation of wave energy conversion devices: A survey," *Applied Energy*, vol. 297, 2021. Cited by: 18; All Open Access, Green Open Access, Hybrid Gold Open Access.

[3] A. Trueworthy and B. Dupont, "The wave energy converter design process: Methods applied in industry and shortcomings of current practices," *Journal of Marine Science and Engineering*, vol. 8, no. 11, p. 1 – 49, 2020. Cited by: 13; All Open Access, Gold Open Access.

[4] M. Folley, A. Babarit, B. Child, D. Forehand, L. O'Boyle, K. Silverthorne, J. Spinneken, V. Stratigaki, and P. Troch, "A review of numerical modelling of wave energy converter arrays," pp. 1–11, 2012.

[5] S. A. Sirigu, G. Bracco, M. Bonfanti, P. Dafnakis, and G. Mattiazzo, "On-board sea state estimation method validation based on measured floater motion," *IFAC-PapersOnLine*, vol. 51, no. 29, pp. 68–73, 2018. 11th IFAC Conference on Control Applications in Marine Systems, Robotics, and Vehicles CAMS 2018.

[6] F. Niosi, L. Parrinello, B. Paduano, E. Pasta, F. Carapellese, and G. Bracco, "On the influence of mooring in wave energy converters productivity: the pewec case," in *2021 International Conference on Electrical, Computer, Communications and Mechatronics Engineering (ICECCME)*, pp. 1–6, 2021.

[7] B. Paduano, G. Giorgi, R. P. Gomes, E. Pasta, J. C. Henriques, L. M. Gato, and G. Mattiazzo, "Experimental validation and comparison of numerical models for the mooring system of a floating wave energy converter," *Journal of Marine Science and Engineering*, vol. 8, no. 8, pp. 1–20, 2020.

[8] A. Babarit and G. Delhommeau, "Theoretical and numerical aspects of the open source bem solver nemoh," *11th European Wave and Tidal Energy Conference (EWTEC2015)*, 2015.

[9] F. Flavià, C. Mcnatt, F. Rongère, A. Babarit, and A. Clément, "Computation of the diffraction transfer matrix and the radiation characteristics in the open-source bem code nemoh," 2016.

[10] J. N. Newman, *Marine hydrodynamics*. MIT Press Cambridge, 1977.

[11] J. C. McNatt, V. Venugopal, and D. Forehand, "The cylindrical wave field of wave energy converters," *International Journal of Marine Energy*, vol. 3-4, pp. e26–e39, 2013. Special Issue – Selected Papers - EWTEC2013.

[12] N. Guillou and G. Chapalain, "Annual and seasonal variabilities in the performances of wave energy converters," *Energy*, vol. 165, pp. 812–823, 2018.

[13] S. A. Sirigu, L. Foglietta, G. Giorgi, M. Bonfanti, G. Cervelli, G. Bracco, and G. Mattiazzo, "Techno-economic optimisation for a wave energy converter via genetic algorithm," *Journal of Marine Science and Engineering*, vol. 8, no. 7, 2020.

[14] M. Bonfanti, S. A. Sirigu, G. Giorgi, P. Dafnakis, G. Bracco, and G. Mattiazzo, "A passive control strategy applied to the iswec device: Numerical modelling and experimental tests," *International Journal of Mechanics and Control*, vol. 21, no. 2, p. 143 – 154, 2020. Cited by: 2.

[15] M. Bonfanti, G. Bracco, P. Dafnakis, E. Giorcelli, B. Passione, N. Pozzi, S. A. Sirigu, and G. Mattiazzo, "Application of a passive control technique to the iswec: Experimental tests on a 1:8 test rig," p. 60 – 70, 2018. Cited by: 11.

[16] P. B. Garcia-Rosa, G. Bacelli, and J. V. Ringwood, "Control-informed optimal array layout for wave farms," *IEEE Transactions on Sustainable Energy*, vol. 6, no. 2, pp. 575–582, 2015.